THE ASTROPHYSICAL JOURNAL, 407:330–341, 1993 April 10


# PHOTOIONIZATION OF THE HYDROGEN ATOM IN STRONG MAGNETIC FIELDS

ALEXANDER YU. POTEKHIN
Department of Theoretical Astrophysics, Ioffe Institute of Physics and Technology, Politekhnicheskaya 26, St. Petersburg, Russia 194021
AND
GEORGE G. PAVLOV[1]
Department of Astronomy, Pennsylvania State University, 525 Davey Laboratory, University Park, PA 16802
*Received 1992 July 7; accepted 1992 October 8*

## ABSTRACT

The photoionization of the hydrogen atom in magnetic fields $B \sim 10^{11}$–$10^{13}$ G typical of the surface layers of neutron stars is investigated analytically and numerically. We consider the photoionization from various tightly bound and hydrogen-like states of the atom for photons with arbitary polarizations and wave-vector directions. It is shown that the length form of the interaction matrix elements is more appropriate in the adiabatic approximation than the velocity form, at least in the most important frequency range $\omega \ll \omega_B$, where $\omega_B$ is the electron cyclotron frequency. Use of the length form yields nonzero cross sections for photon polarizations perpendicular to the magnetic field at $\omega < \omega_B$; these cross sections are the ones that most strongly affect the properties of the radiation escaping from an optically thick medium, e.g., from the atmosphere of a neutron star. The results of the numerical calculations are fitted by simple analytical formulae.

*Subject headings:* atomic processes — magnetic fields — radiation mechanisms: miscellaneous — stars: neutron

## 1. INTRODUCTION

In the typical neutron star magnetic fields $B \sim 10^{11}$–$10^{13}$ G the electron cyclotron energy $\hbar\omega_B = \hbar eB/m_e c$ exceeds significantly the Coulomb energy (i.e., $\beta = \hbar\omega_B/4$ Ry $= B/4.7 \times 10^9$ G $\gg 1$), and the magnetic effects change drastically both the atomic structure and the cross sections of radiative processes (see, e.g., Garstang 1977; Canuto & Ventura 1977). One of the most important radiative processes in neutron star atmospheres is the photoionization of atoms and ions. Since the gravity is very high in the atmospheres, gravitational separation may be very important, and the lightest element present (in particular, hydrogen) may give the main contribution to the opacity of the surface layers. On the other hand, the relative simplicity of the hydrogen atom allows one to investigate all the necessary details of the photoionization process.

The photoionization of the hydrogenic ions in strong magnetic fields has been considered in a number of papers. Approximate analytical investigations of the photoionization cross section at $\ln\beta \gg 1$ were carried out by Hasegawa & Howard (1961) and Gnedin et al. (1974). Hasegawa & Howard considered only the case when the incident photon is circularly polarized, with the wave vector along the magnetic field, and the absorbing atom is on the ground level. Gnedin et al. estimated the cross sections in the Born approximation, which is justified when the photon energy is much higher than the electron binding energy (roughly, at $\hbar\omega \gg [\ln\beta]^2$ Ry). Schmitt et al. (1981) and Wunner et al. (1983b) presented numerical results on the photoionization cross section from the ground state and obtained asymptotic formulae at high photon energies. In the version of the adiabatic approximation they used, the cross section for the photons polarized perpendicular to the field vanishes identically in the most important frequency range $\omega < \omega_B$, in disagreement with other papers, and their high-energy asymptotic expressions differ from those of Hasegawa & Howard (1961) and Gnedin et al. (1974). The cross sections from different levels were computed also by Miller & Neuhauser (1991), without details of the frequency and polarization dependences of the cross sections. Finally, much research has been done recently on the photoionization in moderate magnetic fields, $B \sim 10^7$–$10^9$ G (Kara & McDowell 1981; Greene 1983; Bhattacharya & Chu 1985; Alijah, Hinze, & Broad 1990; Delande, Bommier, & Gay 1991). Kara & McDowell emphasized the importance of modifications of the radial wave functions by Coulomb forces, while the other authors concentrated on the analysis of resonances associated with excitation of metastable levels. In very strong magnetic fields such resonances are tightly grouped near and below the Landau thresholds $\omega = N\omega_B$ ($N \geq 1$) and seem to play only a minor role in the formation of spectra.

The results of the above-cited papers contradict each other in some important points, which obviously must be resolved before one attempts an adequate investigation of the radiative transfer in the atmospheres of strongly magnetized neutron stars. In particular, one should bear in mind that the propagation of radiation in anisotropic atmospheres involves two so-called normal waves (polarization modes) which differ in the polarizations and, as a consequence, in the absorption coefficients and photon mean free paths (Gnedin & Pavlov 1974). Especially important in the radiative transfer is the mode with the *lower* absorption coefficient, because it determines the effective mean free path. Concerning the photoionization, this means that an evaluation of the cross sections for *polarized* radiation is necessary, and the (so far) most discrepant cross sections for photons polarized perpendicular to the field may be of principal importance.

In the present paper, we study analytically and numerically the photoionization in strong magnetic fields of the hydrogen atom in the ground and various excited states. The cross sections are computed and analyzed in a wide frequency range and for different polarizations of the incident photon. The basic equations are presented in § 2. In § 3 we derive and

[1] On leave from Ioffe Institute of Physics and Technology, St. Petersburg, Russia.

discuss asymptotic expressions for the cross sections near the ionization thresholds and at high frequencies. Numerical results and their fitting by simple equations are presented in § 4. In § 5 we briefly discuss applications of the results to the problem of radiative transfer in the atmospheres of neutron stars.

## 2. BASIC EQUATIONS

Let us consider a hydrogen atom placed in a homogeneous magnetic field $\boldsymbol{B}$ directed along the $z$-axis. According to Gor'kov & Dzialoshinskii (1967) and Herold, Ruder, & Wunner (1981), the coordinate part of the wave function of the atom can be written as

$$\Psi(\boldsymbol{r}, \boldsymbol{R}) = \exp\left[i\boldsymbol{K}\boldsymbol{R} - \frac{ie}{2\hbar c}(\boldsymbol{B}\times\boldsymbol{R})\cdot\boldsymbol{r}\right]\psi_{\boldsymbol{K}}(\boldsymbol{r}) , \tag{1}$$

where $\boldsymbol{R} = M^{-1}(m_e\boldsymbol{r}_e + m_p\boldsymbol{r}_p)$ and $\boldsymbol{r} = \boldsymbol{r}_e - \boldsymbol{r}_p$ are the center-of-mass and relative coordinates; $m_e$, $m_p$, and $M = m_e + m_p$ are the electron, proton, and total mass; $-e$ is the electron charge; and $\hbar\boldsymbol{K}$ is the eigenvalue of the generalized momentum of the atom,

$$\boldsymbol{P} = -i\hbar\nabla_{\boldsymbol{R}} - \frac{e}{2c}\boldsymbol{B}\times\boldsymbol{r} . \tag{2}$$

The wave function of the relative motion, $\psi_{\boldsymbol{K}}(\boldsymbol{r})$, obeys the Schrödinger equation with the Hamiltonian

$$H_{\boldsymbol{K}} = \frac{\hbar^2K^2}{2M} + \frac{e\hbar}{Mc}(\boldsymbol{K}\times\boldsymbol{B})\cdot\boldsymbol{r} + \frac{\pi^2}{2\mu} + \frac{e^2}{2Mc^2}(\boldsymbol{B}\times\boldsymbol{r})^2 + V_c(r) , \tag{3}$$

where

$$\pi = -i\hbar\nabla_{\boldsymbol{r}} + \frac{e}{2c}\frac{m_p - m_e}{M}\boldsymbol{B}\times\boldsymbol{r} \tag{4}$$

is the kinetic momentum operator, $V_c(r) = -e^2/r$ is the Coulomb potential, and $\mu = m_e m_p/M$ is the reduced mass.

Up to now the structure of the hydrogen atom has been investigated in detail for $\boldsymbol{K} = 0$ only (fixed atom). Traditional approach to this problem looks as follows (see, e.g., Garstang 1977; Canuto & Ventura 1977; and references therein). Let us expand eigenfunctions $\psi(\boldsymbol{r}) = \psi(\rho, \phi, z)$ of the Hamiltonian (3) with $\boldsymbol{K} = 0$ in terms of the Landau states

$$\Phi_{Ns}(\rho, \phi) = (2\pi)^{-1/2}\exp(-is\phi)a_L^{-1}I_{N+s,N}(\rho^2/2a_L^2) \tag{5}$$

which are the transverse parts of the electron wave functions in the absence of the Coulomb field. In this equation

$$I_{N'N}(\xi) = (-1)^{N'-N}I_{NN'}(\xi) = \frac{1}{\sqrt{N!\,N'!}}e^{\xi/2}\xi^{(N-N')/2}\frac{d^N}{d\xi^N}(\xi^{N'}e^{-\xi}) \tag{6}$$

is the Laguerre function (Sokolov & Ternov 1968; Kaminker & Yakovlev 1981), $N = 0,1,2,\ldots$ is the number of the Landau level, $s = -N, -N+1, \ldots$ is negative of the $z$-projection of the relative angular momentum (in units of $\hbar$), $a_L = (\hbar c/eB)^{1/2} = a_B(2\beta)^{-1/2}$ is the magnetic length, $B = \hbar\omega_B/4$ Ry $= \hbar^3B/2m_e^2c^2e^3$, and $a_B$ is the Bohr radius. For sufficiently large $\beta$, the so-called *adiabatic approximation* is valid, i.e., one term in this expansion exceeds significantly all the others (see, e.g., Simola & Virtamo 1978):

$$\psi(\boldsymbol{r}) = \psi^{ad}_{Ns}(\boldsymbol{r}) + \delta\psi_{Ns}(\boldsymbol{r}) \approx \psi^{ad}_{Ns}(\boldsymbol{r}) , \tag{7}$$

$$\psi^{ad}_{Ns}(\boldsymbol{r}) = \Phi_{Ns}(\rho, \phi)g_{Ns}(z) ; \tag{8}$$

$$\delta\psi_{Ns}(\boldsymbol{r}) = \sum_{N'\neq N}\Phi_{N's}(\rho, \phi)h^{Ns}_{N'}(z) . \tag{9}$$

The wave function $\psi^{ad}_{Ns}(\boldsymbol{r})$ obeys the Schrödinger equation with

$$V_{Ns}(z) = \langle\Phi_{Ns}|\,V_c(r)\,|\Phi_{Ns}\rangle = -\frac{e^2}{a_L\sqrt{2}}\,v_{Ns}\left(\frac{z}{a_L\sqrt{2}}\right) \tag{10}$$

substituted for the real three-dimensional potential. The longitudinal wave function $g_{Ns}(z)$ obeys the one-dimensional Schrödinger equation with the potential (10) and (longitudinal) energy $\epsilon = E - [N + \frac{1}{2} + m_\sigma + (m_e/m_p)(N + s + \frac{1}{2})]\hbar\omega_B$, where $E$ is the total energy, and $m_\sigma = \pm\frac{1}{2}$ is the electron spin projecion on the $z$-axis. Hereafter we shall take into account only the states with $m_\sigma = -\frac{1}{2}$, because, at the field strengths under consideration, contribution of the spin-flip transitions to the photoionization cross sections is several orders of magnitude less than that from corresponding transitions with conserved spin projections (see, e.g., Wunner et al. 1983b).

Negative eigenvalues of the longitudinal energy form a discrete spectrum, $\epsilon = -\epsilon_{Nsn}$, where $n = 0,1,2,\ldots$ counts the nodes of the eigenfunction $g_{Nsn}(z)$ with the parity $(-1)^n$. At $\beta\to\infty$ the energies of the *tightly bound* states ($n = 0$) grow logarithmically, $\epsilon_{Ns0}\sim(\ln\beta)^2$ Ry, whereas the energies of the *hydrogen-like* states ($n \geq 1$) group about the levels of the field-free hydrogen atom, $\epsilon_{Nsn}\to\{\mathrm{Int}\,[(n+1)/2]\}^{-2}$ Ry, where Int ($x$) is the integer part of $x$. All the discrete levels corresponding to $N \geq 1$ are essentially metastable at $\beta \gg 1$, with a typical width $\sim N\alpha^3\beta^2$ Ry, due to natural (radiative) broadening (Wunner et al. 1983a).

Corrections to the adiabatic approximation for the energy levels and bound-bound transition rates were taken into account by Simola & Virtamo (1978), Rösner et al. (1984), and Forster et al. (1984). The deviations of their results from the adiabatic ones appeared to be less than 1% for $\beta > 50$. This allows us to hope that at such high $\beta$ the adiabatic approximation should give a satisfactory accuracy for the photoionization cross sections also.

Let us turn now to the photoionization of the hydrogen atom in a bound state $i$ by a photon with the wave vector $\boldsymbol{q}$ ($|\boldsymbol{q}| = \omega/c$) and polarization unit vector $\boldsymbol{e}$. According to equation (A3), general expression for the cross section summed over the final generalized momenta of the atom reads

$$\sigma_i(\boldsymbol{K}_i) = \frac{4\pi^2e^2\omega}{c}\int d\boldsymbol{K}_f\sum_f|\boldsymbol{D}\cdot\boldsymbol{e}|^2 \times\delta(E_f - E_i - \hbar\omega)\,\delta(\boldsymbol{K}_f - \boldsymbol{K}_i - \boldsymbol{q}) . \tag{11}$$

In the present paper we consider atoms with $\boldsymbol{K}_i = 0$ only. In this case one can neglect the atomic motion in the final states also if the energy of the motion $\sim\hbar^2q^2/2M$ is much less than a typical binding energy $\sim$Ry, i.e., $\hbar\omega \ll (Mc^2\mathrm{Ry})^{1/2} \simeq 100$ keV. Then the cross section can be transformed to the form

$$\sigma_{Nsn} = \sum_{\mu,\nu=-1}^{1}e_\mu e_\nu^*\sigma^{\mu\nu}_{Nsn} = \sum_{\mu,\nu=-1}^{1}e_\mu e_\nu^*\sum_{N_fs_f}\sigma^{\mu\nu}_{Nsn\to N_fs_f} , \tag{12}$$

$$\sigma^{\mu\nu}_{Nsn\to N_fs_f} = \pi\alpha D_{-\mu}D^*_{-\nu}\frac{\hbar\omega}{\sqrt{\epsilon_f\,\mathrm{Ry}}}\frac{L}{a_B} , \tag{13}$$

where $e_0 = e_z$, $e_{\pm 1} = (e_x \pm ie_y)/\sqrt{2}$, $\alpha = e^2/\hbar c$, $L$ is the $z$-extension of the periodicity volume of the final state, and

$$\epsilon_f = \hbar\omega - \epsilon_{Nsn} - [(N_f - N)(1 + m_e/m_p) + (s_f - s)m_e/m_p]\hbar\omega_B \quad (14)$$

is the longitudinal energy (hereafter we shall omit the subscript $i$ for the initial states). Since the states with $N > 0$ are metastable and almost unpopulated in the high magnetic fields, we adopt $N = 0$. Then the threshold photon energy for fixed $N$ and $s$ is

$$\hbar\omega^{(t)}_{N_f s_f} = \epsilon_{0sn} + [N_f(1 + m_e/m_p) + (s_f - s)m_e/m_p]\hbar\omega_B . \quad (15)$$

Note that the term $(s_f - s)m_e/m_p$ is by no means negligible, at least at $N_f = 0$, as it may be comparable with the binding energy $\epsilon_{0sn}$ (cf. Herold et al. 1981).

The cross sections evaluated with the aid of approximate wave functions may essentially depend on the choice of the form of the matrix element $\boldsymbol{D}$. For instance, Schmitt et al. (1981), Wunner et al. (1983b), and Mega et al. (1984) used the *velocity form* and obtained zero cross section for the transverse polarizations $\mu = \pm 1$ at $\omega < \omega^{(t)}_{1s_f}$. On the other hand, Hasegawa & Howard (1961), Gnedin et al. (1974), and Miller & Neuhauser (1991) used the *length form* and obtained finite cross sections in the same frequency range. General expressions and various approximations for the matrix element $\boldsymbol{D}$ are discussed in Appendix A. It is shown there that if one calculates $\boldsymbol{D}$ with the adiabatic wave functions, the length form of the matrix element is preferable, at least in the most important case $\omega \ll \omega_B$. Thus, neglecting the corrections $\sim m_e/m_p$ in the matrix elements, we use (cf. eq. [A7])

$$\boldsymbol{D} = \langle \Phi_{N_f s_f} g_{N_f s_f \epsilon_f} | e^{iqr} \times r\left(1 - \frac{\hbar\omega}{2m_e c^2} - \frac{\boldsymbol{q}\cdot\boldsymbol{\pi}}{|\boldsymbol{q}|\, m_e c}\right) | \Phi_{0s}\, g_{0sn}\rangle \quad (16)$$

The matrix element $\boldsymbol{D}$ can be expressed in terms of the Laguerre functions (see eq. [6]) with the aid of the following relations

$$r_{+1}\Phi_{Ns} = a_L(\sqrt{N + s}\,\Phi_{N,s-1} - \sqrt{N+1}\,\Phi_{N+1,s-1}) , \quad (17)$$

$$r_{-1}\Phi_{Ns} = a_L(\sqrt{N + s + 1}\,\Phi_{N,s+1} - \sqrt{N}\,\Phi_{N-1,s+1}) , \quad (18)$$

$$\pi_{+1}\Phi_{Ns} = -\frac{i\hbar}{a_L}\sqrt{N+1}\,\Phi_{N+1,s-1} , \quad (19)$$

$$\pi_{-1}\Phi_{Ns} = \frac{i\hbar}{a_L}\sqrt{N}\,\Phi_{N-1,s+1} , \quad (20)$$

and (Sokolov & Ternov 1968)

$$\int_0^\infty J_{s_f - s}(2\sqrt{u\xi}) I_{N_f + s_f, N_f}(\xi) I_{N+s,N}(\xi) d\xi = I_{N_f + s_f, N+s}(u) I_{N_f N}(u) , \quad (21)$$

where $J_l(x)$ is a Bessel function. These relations yield

$$D_0 = I_{N_f + s_f, s}(u)[I_{N_f 0}(u)Z_1^{\parallel} + I_{N_f 1}(u)Z_1^{\perp}] , \quad (22)$$

$$D_{+1} = a_L\{I_{N_f+s_f,s-1}(u)\sqrt{s}\,[I_{N_f0}(u)Z_0^{\parallel} + I_{N_f1}(u)Z_0^{\perp}] - I_{N_f+s_f,s}[I_{N_f1}(u)Z_0^{\parallel} + \sqrt{2}\,I_{N_f2}(u)Z_0^{\perp}]\} , \quad (23)$$

$$D_{-1} = a_L\{I_{N_f+s_f,s+1}(u)\sqrt{s+1}\,[I_{N_f0}(u)Z_0^{\parallel} + I_{N_f1}(u)Z_0^{\perp}] - I_{N_f+s_f,s}(u)I_{N_f0}(u)Z_0^{\perp}\} , \quad (24)$$

where $u = (qa_L \sin\theta)^2/2 = (\hbar\omega/2m_e c^2)(\omega/\omega_B)\sin^2\theta$, $\theta$ is the angle between $\boldsymbol{q}$ and $\boldsymbol{B}$, $\boldsymbol{q}$ lies in the $(y, z)$-plane, and

$$Z_k^{\parallel} = \langle g_f | e^{iqz\cos\theta} z^k \times \left(1 - \frac{\hbar\omega}{2m_e c^2} + i\cos\theta\sqrt{\frac{\hbar\omega_B}{m_e c^2}}\, a_L \frac{\partial}{\partial z}\right) | g\rangle , \quad (25)$$

$$Z_k^{\perp} = \sin\theta\sqrt{\frac{\hbar\omega_B}{2m_e c^2}}\,\langle g_f | e^{iqz\cos\theta} z^k | g\rangle . \quad (26)$$

The terms proportional to $\hbar\omega/m_e c^2$ and $(\hbar\omega_B/m_e c^2)^{1/2} \sim \alpha(\beta)^{1/2}$ originate from the second and third terms in the parentheses of equation (16). They give only small corrections to $Z_k^{\parallel}$ ($\sim \hbar\omega/m_e c^2$ and $\sim \alpha \ln\beta \cos\theta$, respectively). On the other hand, the terms proportional to $Z_k^{\perp}$ (being of the same origin) may make substantial contribution to the matrix elements at $\omega > \omega^{(t)}_{1s_f}$.

Equations (22)–(24) simplify significantly in some limiting cases. They look especially simple for $\theta = 0$,

$$D_{+1} = \delta_{s_f, s-1}(\delta_{N_f 0}\sqrt{s} - \delta_{N_f 1})a_L Z_0^{\parallel} , \quad (27)$$

$$D_{-1} = \delta_{s_f, s+1}\,\delta_{N_f 0}\sqrt{s+1}\,a_L Z_0^{\parallel} \quad (28)$$

($D_0$ does not contribute to the cross section because $\boldsymbol{e}\cdot\boldsymbol{q} = 0$). This means, in particular, that at

$$\omega < \omega^{(t)}_{1,-1} \simeq \omega_B$$

the cross section vanishes identically for the circular polarization $\boldsymbol{e} = \boldsymbol{e}_{-1}$ if the atom is in any state with $s = 0$, including the ground one (cf. Gnedin et al. 1974). Note that the last statement follows from the conservation of the angular momentum and energy, so it remains correct outside the framework of the adiabatic approximation.

Equations (22)–(24) are also simplified in the dipole approximation. Since $z$-extension of the atom in the magnetic field is larger than its transverse size, one can distinguish the transverse dipole approximation (Wunner et al. 1983b). Being valid at $\hbar\omega \sin\theta \ll \alpha(\beta)^{1/2} m_e c^2$, it corresponds to replacing in these equations all the functions $I_{N_1 N_2}(u)$ by $\delta_{N_1 N_2}$. More restrictive is the longitudinal dipole approximation [$\exp(iqz\cos\theta) \to 1$] valid at

$$\hbar\omega\cos\theta \ll \sqrt{m_e c^2 \cdot \epsilon_{0sn}} .$$

Thus, equations (12), (13), and (22)–(24) allow one to evaluate the photoionization cross section at $\hbar\omega$, $\hbar\omega_B \ll m_e c^2$ for arbitrary photon polarizations and angles of incidence.

## 3. ANALYTICAL RESULTS FOR VERY HIGH $\beta$

Equations (22)–(26) reduce the problem to evaluating the longitudinal matrix elements (overlap integrals) $Z_k$. In the limit of very strong magnetic field ($\ln\beta \gg 1$), the evaluation can be done analytically for some particular cases.

The longitudinal wave functions obey the following equation

$$\left[\frac{d^2}{d\zeta^2} + \frac{2}{\sqrt{\beta}}\, v_{Ns}(\zeta) + \frac{\epsilon}{\beta}\right] g(\zeta) = 0 , \quad (29)$$

where $\zeta = \sqrt{2}\, z/a_L$, $v_{Ns}(\zeta)$ is defined by equation (10), and $\epsilon$ is the longitudinal energy in Ry. An efficient method for solving this equation and evaluating the cross section in the dipole

approximation for the transverse polarizations ($\mu, \nu = \pm 1$) has been presented by Hasegawa & Howard (1961). They suggested to neglect the last term in equation (29) at $|\zeta| \leq \zeta_0$ (where a matching pont $\zeta_0$ obeys the inequality $1 \ll \zeta_0 \ll \beta^{1/2}$), to replace the potential by its asymptotic expression [$v_{Ns}(\zeta) \sim \zeta^{-1}$] at $|\zeta| > \zeta_0$, and to evaluate $\langle g_f | g \rangle$ approximately as an overlap integral over the region $\zeta_0 < |\zeta| < \infty$. The method was originally applied to the ground initial state of the atom. For transitions from arbitrary even states $\{0, s, n\}$ with $n = 0,2, 4, \ldots$ to continuum states $\{0, s_f \geq 0, \epsilon_f\}$ with $\epsilon_f = \hbar\omega - \epsilon_{0sn} - (s_f - s)(m_e/m_p)\hbar\omega_B$, we obtain

$$\sigma^{\mu\mu}_{0sn\to 0s_f} = \frac{4\pi^2\alpha a_B^2}{\beta}\frac{\hbar\omega}{\mathrm{Ry}}\,\delta_{s_f,s+\mu}\,\frac{C_{sn}}{s+(1+\mu)/2}\,\frac{Y}{(\epsilon_f+\epsilon_{0sn})^2} \times \{4\pi^2 + Y^2[X_{s_f} - \ln\epsilon_f - 2\,\mathrm{Re}\,\psi(1+i\epsilon_f^{-1/2})]^2\}^{-1}, \quad (30)$$

where $\mu = \pm 1$, $\psi(x) = (d/dx)\ln\Gamma(x)$, $C_{s0} = (\epsilon_{0s0})^{1/2}$,

$$C_{sn} = 2\epsilon_{0sn}^{3/2}(4\pi^2 + X_s^2)^{-1}, \quad n = 2,4, \ldots$$

$$Y = 1 - \exp(-2\pi\epsilon_f^{-1/2}),$$

$$X_s = \ln\beta - 3\gamma - \sum_{k=1}^{s} k^{-1}$$

(the sum here and in eqs. [31], [33], and [34] is to be replaced by zero for $s = 0$). The energy eigenvalues $\epsilon_{0sn}$ can be obtained either by numerical solving equation (29) or from the simpler equations

$$\sqrt{\epsilon_{0s0}} + \ln\epsilon_{0s0} = \ln\beta - \gamma - \sum_{k=1}^{s} k^{-1}, \quad (31)$$

and

$$\epsilon_{0sn} = \left(\frac{n}{2} + \delta_n\right)^{-2}, \quad n = 2,4, \ldots \quad (32)$$

$$\delta_n = 2\left(\ln\beta - 3\gamma - \sum_{k=1}^{s} k^{-1} + \frac{2}{3n^2}\right)^{-1}. \quad (33)$$

Note that the effect of the finite proton mass may shift significantly the threshold frequency

$$\omega^{(t)}_{0,s+\mu} = \epsilon_{0sn}/\hbar + \mu(m_e/m_p)\omega_B.$$

Moreover, $\omega^{(t)}_{0s_f}$ may become negative for $\mu = -1$ for sufficiently high fields, which means that the physical threshold is shifted to $\omega = 0$, where the cross section equals zero.

Since $g_f(\epsilon_f \to 0, \zeta = 0) \propto \epsilon_f^{-1/4}$, the divergent factor $\epsilon_f^{-1/2}$ in equation (13) is compensated, and the cross section near the threshold $\omega^{(t)}_{0,s+\mu} > 0$ is finite,

$$\sigma^{\mu\mu}_{0sn\to 0s_f}[\omega = \omega^{(t)}_{0,s+\mu}] = 1.2\times 10^7\sigma_T\,\frac{[\hbar\omega^{(t)}_{0,s+\mu}/\mathrm{Ry}]C_{sn}}{\beta[s+(1+\mu)/2]\epsilon_{0sn}^2} \times \left\{39.5 + \left(\ln\beta - 1.73 - \sum_{k=1}^{sf} k^{-1}\right)^2\right\}^{-1}\delta_{s_f,s+\mu}, \quad (34)$$

where $\sigma_T = (8\pi/3)(e^2/mc^2)^2$ is the Thomson cross section. The factor $1/\beta$ corresponds to the reduction of the transverse atomic size by $\sim\beta^{1/2}$ in a strong magnetic field whereas the factor $\sim(\ln\beta)^{-2}$ is due to behavior of the continuum wave function at $\zeta \to 0$. An additional decrease of the cross section for $n = 0$ occurs with increasing $\beta$ due to growth of the ionization energy $\epsilon_{0s0} \propto (\ln\beta)^2$.

Let us consider now the behavior of $\sigma(\omega)$ at high $\omega$. Equation (30) yields $\sigma^{\mu\mu} \propto \omega^{-3/2}$ at $\omega \gg \omega^{(t)}_{0s_f}$, in accordance with the result of Gnedin et al. (1974). On the other hand, an asymptotic expression in the Born approximation can be obtained by substituting $g_f(\zeta) = L^{-1/2}\exp[i(\epsilon_f/\beta)^{1/2}\zeta]$ into equation (A13), performing the successive partial integrations, and expanding the result in the power series of $\epsilon_f^{-1/2}$. This approach was used by Schmitt et al. (1981) for $s = 0$. For arbitrary $s$, we obtain

$$\sqrt{\frac{2}{L}}\int_{-\infty}^{\infty}\cos\left(\sqrt{\frac{\epsilon_f}{\beta}}\,\zeta\right)g_{0sn}(\zeta)d\zeta = (-1)^s\sqrt{\frac{32}{\beta L}}\,g_{0sn}(0) \times\left[\frac{d^{2s+1}}{d\zeta^{2s+1}}\,v_{0s}(\zeta)\right]_{\zeta=0}, \quad (35)$$

which gives for $\mu = \pm 1$

$$\sigma^{\mu\mu}_{0sn\to 0s_f} \simeq \frac{3}{2\alpha^3}\,\sigma_T\,\delta_{s_f,s+\mu}\left[s + \frac{\mu+1}{2}\right] \times (s!)^2(4\beta)^{2s+3/2}\,|g_{0sn}(0)|^2\left(\frac{\mathrm{Ry}}{\hbar\omega}\right)^{2s+7/2}. \quad (36)$$

Differentiating equation (35) with respect to $\epsilon_f^{-1/2}$ yields

$$\sigma^{00}_{0sn\to 0s_f} \simeq \frac{3}{2\alpha^3}\,\sigma_T\,\delta_{s_f s}(s+2)^2 \times (s!)^2(4\beta)^{2s+5/2}\,|g_{0sn}(0)|^2\left(\frac{\mathrm{Ry}}{\hbar\omega}\right)^{2s+9/2}. \quad (37)$$

Equations (36) and (30) are in obvious contradiction caused by difference of their validity ranges. The approximations used to derive equation (30) (in particular, neglecting the last term in eq. [29]) are invalid when $\epsilon_f \gtrsim \beta^{1/2}$. On the other hand, the terms neglected in equation (35) are small at $\hbar\omega \gg 4\beta\mathrm{Ry} = \hbar\omega_B$. Thus, the asymptotic behavior $\omega^{-3/2}$ takes place in the range $\hbar\omega^{(t)}_{0s_f} \ll \hbar\omega \ll \beta^{1/2}$ Ry, which exists at sufficiently high $\beta$, whereas equations (36) and (37) are valid at extremely high $\omega$, where the transitions to higher Landau levels give larger contribution to the total cross section than the transition to $N_f = 0$ considered here.

## 4. NUMERICAL RESULTS

The photoionization cross sections were computed with the aid of equations (22)–(26). Some technicalities of the computation are described in Appendix B.

Figure 1 shows the partial cross sections $\sigma^{\mu\mu}_{0sn\to 0s_f}$ as a function of the final longitudinal energy $\epsilon_f$ at several values of the magnetic field $B$ for the photons with the right circular polarization at $\theta = 0°$ and the linear polarization parallel to $\boldsymbol{B}$ at $\theta = 90°$. The comparison of the numerical cross sections (*solid curves*) with the approximation (30), (36), and (37) plotted by dashed and dotted curves shows that, in accordance with the conclusions of § 3, equation (30) gives fairly good results at low and medium $\epsilon_f$, especially for the tightly bound initial states, whereas the asymptotic curves (36) and (37) are close to numerical ones at $\epsilon_f \simeq \hbar\omega \gg \hbar\omega_B$ only. The cross sections for the transverse polarizations are much smaller (by a factor of the order of $\beta$) than for the longitudinal polarization at $\omega \ll \omega_B$ due to transverse magnetic compression of the atom. Growth

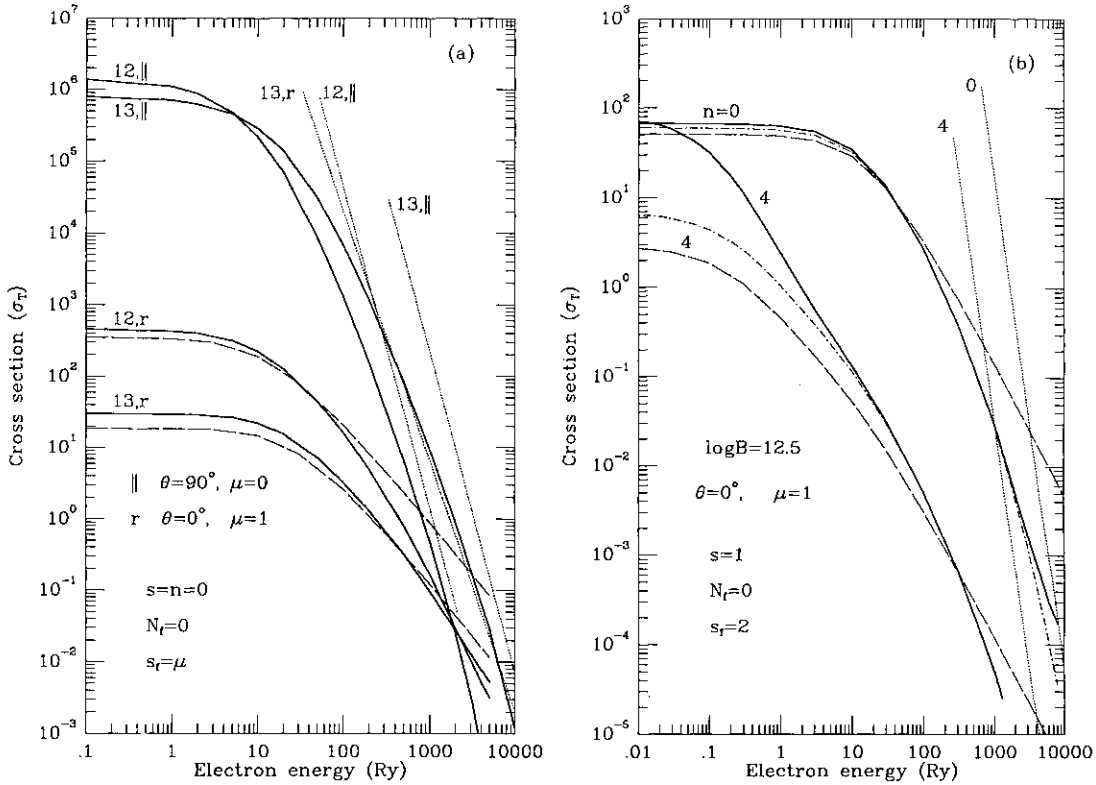


FIG. 1.—Partial cross section $\sigma^{\mu\mu}_{0ns\to 0,s+\mu}$ vs. final longitudinal electron energy for different magnetic fields, photon incident angles, and polarizations. Solid, long-dashed, and dotted curves show numerical results (eqs. [22]–[26]), analytical approximation (eq. [30]), and high-energy asymptotes (eq. [35] and [36]), respectively. (*a*) Transitions from the ground state ($s = n = 0$). The curves are labeled by log $B$ (gauss) and symbols ‖ and $r$ which correspond to the longitudinal linear polarization ($\mu = 0$), $\theta = 90°$, and right circular polarization ($\mu = +1$), $\theta = 0°$, respectively. (*b*) Transitions from the excited states $s = 1$, $n = 0$ and 4 (figures near the curves) for $B = 10^{12.5}$ G, $\theta = 0°$, $\mu = +1$. Dash-dotted curves present the numerical results in the dipole, infinite-proton-mass approximation.

of the magnetic field diminishes the cross sections near the thresholds for any given polarization, whereas at high frequencies the cross sections increase with the field. Figure 1*b* demonstrates in addition, an increase of the near-threshold cross sections for $\mu = 1$ (which would turn into a decrease for $\mu = -1$) due to allowance for the finite proton mass in the relation between $\omega$ and $\epsilon_f$ (see eq. [14]), which is the most significant for the hydrogen-like initial levels.

The partial cross sections for the transitions from the ground state to the continuum of the first *excited* Landau level ($N_f = 1$, $s_f = -1$) are shown in Figure 2 for photons with the left circular polarization at $\theta = 0°$ and linear polarizations parallel and perpendicular to the magnetic field at $\theta = 90°$. These transitions are allowed for $\omega > \omega^{(t)}_{1,-1} = \omega_B + \epsilon_{000}/\hbar$. Absorption of the photons with the left polarization, strictly forbidden for transitions from the ground state to states with $N_f = 0$, dominates at $N_f = 1$. The resonances in this absorption are caused by coincidence of the electron and photon wave numbers. In the Born approximation (justified at $\epsilon_f \gg$ Ry) one has $g_f \propto \exp(\pm ik_e z)$, where $k_e = (\epsilon_f/\mathrm{Ry})^{1/2} a_B^{-1}$, $\epsilon_f \approx \hbar(\omega - N_f\omega_B)$. Multiplication of $g_f$ by $\exp(iqz\cos\theta)$ in the matrix elements (25) is equivalent to substitution $k_e + q\cos\theta$ for $k_e$ in the final wave function, with $q = \alpha(\hbar\omega/2\ \mathrm{Ry})a_B^{-1}$. Therefore, a resonance $k_e \approx q\cos\theta$ arises at

$$\epsilon_{f,\mathrm{res}} = [1 - \sqrt{1 - 4(\alpha\cos\theta)^2\beta N_f}]^2(\alpha\cos\theta)^{-2}\ \mathrm{Ry}$$
$$\approx (2\alpha\beta N_f\cos\theta)^2\ \mathrm{Ry}\ . \qquad (38)$$

The resonances are imperceptible, and deviations from the longitudinal dipole approximation play only a minor role, if $\epsilon_{f,\mathrm{res}} \lesssim$ Ry. This is the case, in particular when $N_f = 0$ or $\theta \approx 90°$.

Figure 3 demonstrates frequency dependences of the total cross sections for an atom in the ground state ionized by polarized light at $\theta = 0°$ or $\theta = 90°$, the magnetic field varying from $10^{11.5}$ to $10^{13}$ G. The nonmagnetic cross section from the ground state is also shown for comparison. Absorption of the left-polarized photons (Fig. 3*a*) is allowed only for $\omega > \omega_B + \epsilon_{000}$. The threshold cross sections are by a factor of the order of $\beta$ higher than for right polarization, being comparable with those for longitudinally polarized photons. Note that the maximum of the cross section for $B = 10^{12.5}$ G is slightly shifted from the threshold due to the resonance shown in Figure 2. The sharp peaks in Figure 3*b* correspond to transitions to the excited Landau states, $N_f = 1, 2, \ldots$. They would disappear if we used the dipole approximation. Such peaks do not arise in Figure 3*a* because the only allowed transitions at $\theta = 0°$ are those to $N_f = 0$ and 1 for right and left polarization, respectively.

Figure 4 shows cross sections for transitions from the tightly bound states with various $s$ in the case of linearly polarized photons propagating perpendicular to $\boldsymbol{B}$. The photon energy range is shown where the transitions to $N_f = 0$ are allowed only (i.e., $s_f = 0,1,\ldots$). We see that the maximum cross sections for the longitudinal polarization grow with $s$ slowly, whereas those for the transverse polarization decrease with increasing $s$

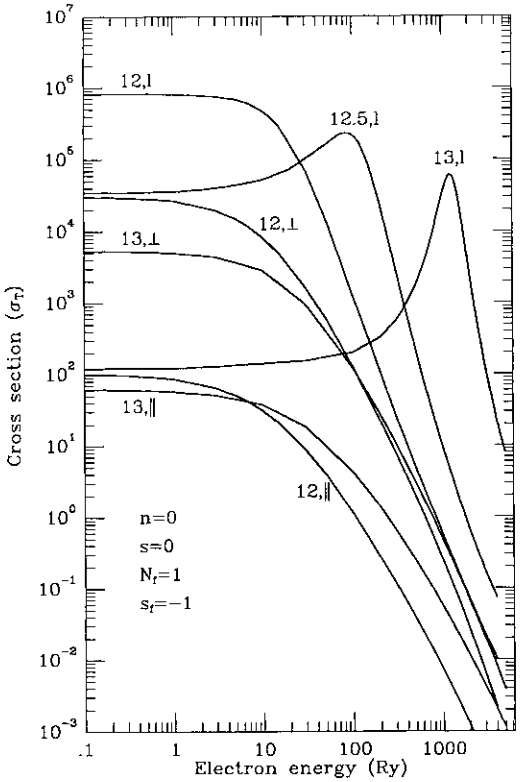


FIG. 2.—Partial cross section for $n = 0$, $s = 0$, $N_f = 1$, $s_f = -1$, and $B = 10^{12}$, $10^{12.5}$, and $10^{13}$ G. Symbols $l$, $\|$, and $\perp$ correspond to the left circular polarization at $\theta = 0°$, longitudinal linear polarization at $\theta = 90°$, and transverse linear polarization at $\theta = 90°$, respectively.

from $s = 1$. These maxima are reached at the "main" thresholds associated with the transitions to $s_f = s$ and $s_f = s + 1$ for the longitudinal and transverse polarizations, respectively. Additional (lower) thresholds are seen for $s \neq 0$. They correspond to $s_f = s - 1$ and are shifted leftward in accordance with equation (15). Transitions to $s_f = s$ and $s_f > s + 1$ are also allowed for transverse polarization but their contributions are so small that the corresponding thresholds do not display on the curves (just as the thresholds for $s_f > s$ on the curves for the longitudinal polarization).

Figures 5 and 6 demonstrate the cross sections for various longitudinal quantum numbers $n$ at several values of $s$. The nonzero cross sections at frequencies below the main thresholds are caused by the transitions to states with $s_f = s - 1$, exactly as the "steps" in Figure 4. The corresponding additional thresholds are shifted, formally, to negative frequencies for all the hydrogen-like states, $n \geq 1$, in the field under consideration, $B = 10^{12.5}$ G. This means that such initial states are metastable, and photoionization is allowed at any (positive) frequencies.

The shapes of the cross section spectra above the main thresholds for the even hydrogen-like states (Fig. 5) strongly resemble those for the tightly bound states. On the contrary, the spectra for the odd states and longitudinally polarized photons show quite different behavior near the main thresholds at $s = 0$ (Fig. 6*a*). Besides, they display sharp dips (Fig. 6*b*). The dips, mentioned previously by Mega et al. (1984), appear at energies where the longitudinal matrix element $Z_1^{\|}$ changes its sign with varying energy. The finite cross sections at these energies are due to the second term in equation (22) which would vanish in the transverse dipole approximation.

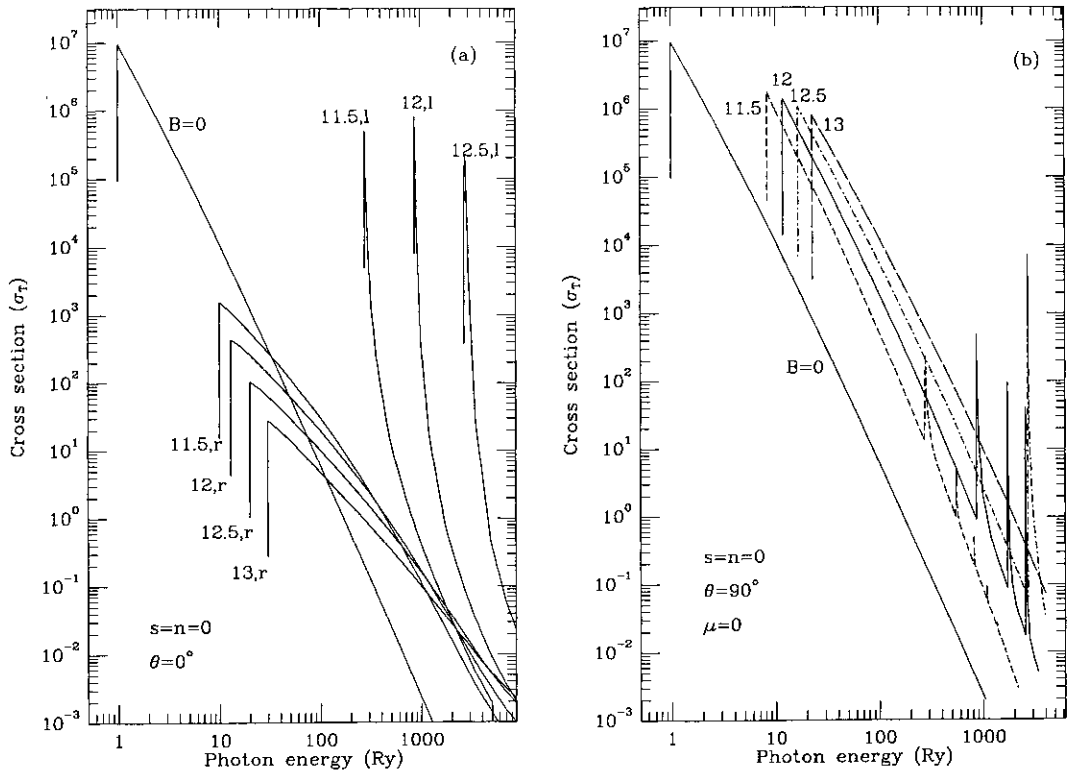


FIG. 3.—Total cross section as a function of the photon energy for the atom in the ground state ($s = n = 0$) and various log $B$ (figures near the curves). (*a*) $\theta = 0°$; right (*r*) and left (*l*) circular polarizations. (*b*) $\theta = 90°$, longitudinal polarization.

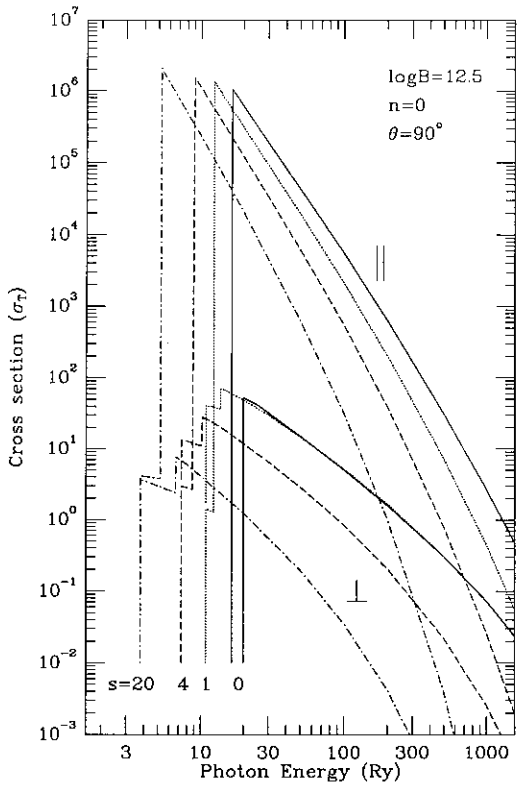


FIG. 4.—Spectra of the total cross sections for various tightly bound initial states $n = 0$, $s = 0,1,4,20$ (figures near the curves) at $B = 10^{12.5}$ G, $\theta = 90°$ for longitudinal (∥) and transverse (⊥) photon polarizations.

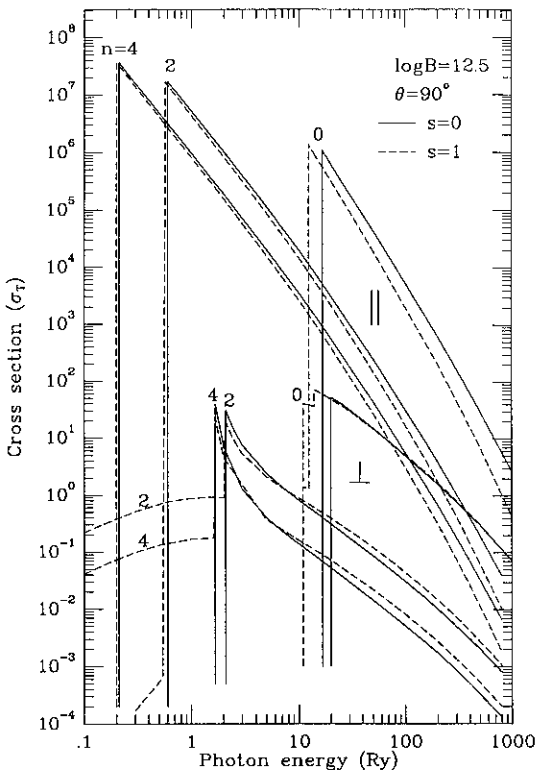


FIG. 5.—Spectra of the total cross sections for longitudinal (∥) and transverse (⊥) polarizations for various even $n$ (figures near the curves) at $B = 10^{12.5}$ G, $\theta = 90°$. Solid and dashed lines correspond to $s = 0$ and $s = 1$, respectively.

The computed cross sections can be fitted by simple equations for the most important case of the tightly bound initial states and not too high photon frequencies, $\omega < \omega_B$, when the transitions to $N_f = 0$ only are important. In particular, making use of equations (30), (36), and (37), we obtain

$$\frac{\sigma^{\mu\mu}_{0s0\to 0,s+\mu}(\omega)}{\sigma^{\mu\mu}_{0s0\to 0,s+\mu}(\omega^{(t)}_{0,s+\mu})} = \left(\frac{\omega}{\omega^{(t)}_{0,s+\mu}}\right)^{|\mu|} \times \frac{1}{(1+a_\mu y)^{2.5}} \frac{1}{[1+b_\mu(\sqrt{1+y}-1)]^{4(s+1)}}, \quad (39)$$

where

$$y = \frac{\epsilon_f}{\epsilon_{0s0}} = \frac{\hbar(\omega - \omega^{(t)}_{0,s+\mu})}{\epsilon_{0s0}}$$

$$a_0 = 1.15\,, \quad a_{+1} = 0.72\,, \quad a_{-1} = 0.69\,,$$

$$b_\mu = c_\mu(1 + d_\mu s)^{-1}\beta^{(|\mu|-3.5)^{-1}}\,,$$

$$c_0 = c_{+1} = 0.69\,, \quad c_{-1} = 0.27\,,$$

$$d_0 = d_{+1} = 0.5\,, \quad d_{-1} = 0.1\,;$$

and (cf. eq. [31])

$$\epsilon_{0s0} = [\ln\beta + a_s - b_s \ln(\ln\beta + c_s)]^2 \text{ Ry}\,,$$

$$a_s = 4.287 + 3.7677\ln(s + 3.604)\,,$$

$$b_s = 3.910 + 1.2859\ln(s + 2.021)\,,$$

$$c_s = 3.709 + \ln(s + 2.38)\,. \quad (40)$$

The threshold values of the cross section in equation (39) can be approximated as (cf. eq. [34])

$$\sigma^{00}_{0s0\to 0s}[\omega^{(t)}_{0s}] = \frac{5.14\times 10^6 \sigma_T (\text{Ry}/\epsilon_{0s0})^{1/2}}{1 + 0.00968(1+\sqrt{s+2})[\ln\beta - 4.87 - \ln(s+0.35)]^2}\,, \quad (41)$$

$$\sigma^{+1\,+1}_{0s0\to 0,s+1}[\omega^{(t)}_{0,s+1}] = 2.25\times 10^5 \sigma_T \frac{\hbar\omega^{(t)}_{0,s+1}}{\epsilon_{0s0}}\left(1 + \frac{1}{\sqrt{s+1}}\right) \times \left(\frac{\text{Ry}}{\epsilon_{0s0}}\right)^{1/2} \frac{1 + 5.5\times 10^{-10}(s+1)^2\beta^2\cos^2\theta}{\beta(s+1+0.0141\ln^2\beta)}\,, \quad (42)$$

$$\sigma^{-1\,-1}_{0s0\to 0,s-1}[\omega^{(t)}_{0,s-1}] = 2.97\times 10^5 \sigma_T \frac{\hbar\omega^{(t)}_{0,s-1}}{\epsilon_{0s0}} \times \left(\frac{\text{Ry}}{\epsilon_{0s0}}\right)^{1/2} \frac{1 + 5.5\times 10^{-10} s^2\beta^2\cos^2\theta}{\beta(s+0.0087\ln^2\beta)}\,, \quad s > 0\,. \quad (43)$$

The typical error of the approximation for the energies (eq. [40]) is about 1%–2% for $0 \le s \le 100$ in the range $50 \le \beta \le 5000$, the maximum error being 4% for high $s$ and low $\beta$. The error of the threshold cross sections (eqs. [41] through [43]) is about 1% for $\mu = 0$ and 3% for $\mu = \pm 1$ at $50 \le \beta \le 5000$, $0 \le s \le 10$. The approximation (39) of the cross sections above the thresholds becomes, generally, the less accurate the lower the cross section value. The typical error in

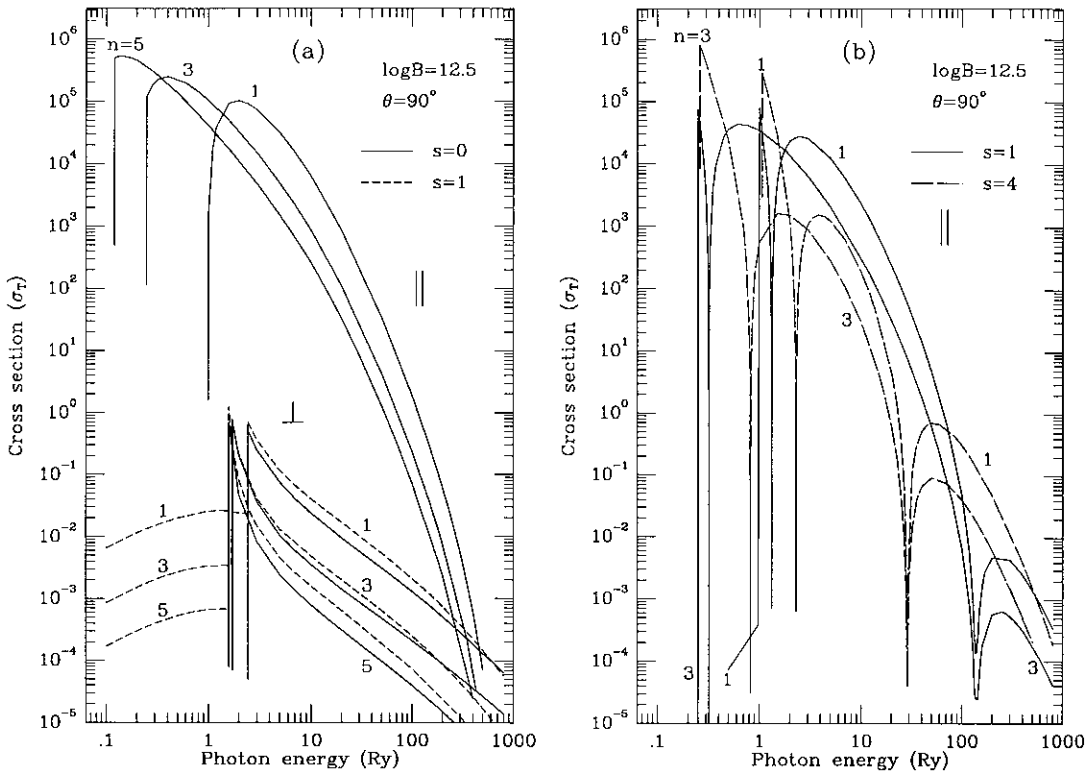


FIG. 6.—Spectra of the total cross sections for odd $n$

those frequency ranges where $\sigma > 10^{-2}\sigma_T$ is $\simeq 6\%$ at $70 \leq \beta \leq 2000$, $0 \leq s \leq 10$. It may reach 15%–30% at high-frequency boundaries of these ranges, where the intrinsic accuracy of the computational results may be even worse.

## 5. DISCUSSIONS AND CONCLUSIONS

The main features of the photoionization process in strong magnetic field, $\beta = \hbar\omega_B/4$ Ry $\gg 1$, can be outlined as follows.

1. Strong magnetic fields qualitatively change the *frequency dependence* of the photoionization cross section. In particular, the thresholds corresponding to the lowest (tightly bound) atomic levels are shifted to substantially higher energies. The cross sections above the thresholds decrease with $\omega$ slower than in the field-free case. Additional thresholds associated with continua of the excited Landau levels $N_f = 1,2,\ldots$ arise at $\omega \gtrsim N_f \omega_B$.

2. The photoionization cross section depends strongly on the *polarization* of the incident radiation. Generally, the cross section at frequencies $\omega \ll \omega_B$ is much larger for photons polarized parallel to the magnetic field. For the longitudinally polarized photons, the magnetic field depresses the maximum (threshold) values of the cross section only slightly whereas the cross sections for transverse polarizations are in addition depressed by a large factor $\sim\beta$, and they decrease with $\omega$ slower than those for the longitudinal polarization. The photoionization from the states $s = 0$ to the continuum of the ground Landau level is strictly forbidden for the "left" circular polarization, with $E$-vector rotating in the same direction as a free electron in a magnetic field. On the other hand, the cross section for the left polarization is much higher than for other polarizations above the first Landau threshold (i.e., at $\omega \gtrsim \omega_B$).

3. Even the polarization-summed cross section is strongly *anisotropic*. In particular, the cross section at $\omega \ll \omega_B$ is much smaller for $\theta = 0$ or $\pi$, i.e., for photons propagating along the magnetic field, than for $\theta = \pi/2$.

4. The behavior of the cross section is different for the tightly bound, even hydrogen-like, and odd hydrogen-like initial levels of the atom. For instance, the peak cross sections for the longitudinal polarization are higher from the even hydrogen-like levels than from the odd and tightly bound levels. Cross sections from the odd states display quite different near-threshold behavior and have deep narrow dips at some frequencies.

In addition to these general properties of the magnetic photoionization, partly known from previous publications (Hasegawa & Howard 1961; Gnedin et al. 1975; Schmitt et al. 1981; Wunner et al. 1983a), we also showed that the length form of the interaction matrix element is more appropriate in the adiabatic approximation than the velocity form in the most important frequency range $\omega \ll \omega_B$ ($\hbar\omega \ll$ 1–100 keV for $B = 10^{11}$–$10^{13}$ G). In particular, applying this form provides nonzero cross sections for transverse polarizations at $\omega < \omega_B$. We also found that different forms for the partial cross sections obtained by Hasegawa & Howard (1961) and Gnedin et al. (1975), on the one hand, and Schmitt et al. (1981) and Wunner et al. (1983b), on the other hand, are valid in different frequency regions (Ry/$\hbar \ll \omega \ll \omega_B$ and $\omega \gg \omega_B$, respectively). We first took into account the effect of the finite proton mass on the photoionization. It leads to an additional shift, $\Delta\omega = \Delta s(m_e/m_p)\omega_B$, of the threshold corresponding to a transition to $s_f = s + \Delta s$. This means, in particular, that the thresholds for the right and left circular polarizations are shifted to higher and lower energies, respectively; in the latter case the thresholds can be even shifted (formally) to negative frequencies which reflects the fact that the boundary of the continuum corresponding to $s_f = s - 1$ lies lower than the energy of the

initial (metastable) level. Since we considered the photoionization outside the framework of the dipole approximation (i.e., the transitions with $|\Delta s| > 1$ are allowed), the effect of the finite proton mass is also displayed in a "stairlike" structure of the thresholds of the total cross section (see, e.g., Fig. 4).

To apply the results to astrophysical problems one should evaluate the absorption coefficients (opacities) of the so-called normal waves (polarization modes) reponsible for transfer of radiation in optically thick, anisotropic media (see, e.g., Gnedin & Pavlov 1974). The absorption coefficients can be expressed through the cross sections as

$$k_j = \sum_{\mu,\nu=-1}^{1} k_{\mu\nu} e^j_\mu e^{j*}_\nu = \sum_{s,n} \mathcal{N}_{sn} \sum_{\mu,\nu=-1}^{1} e^j_\mu e^{j*}_\nu \sigma^{\mu\nu}_{0sn} , \quad (44)$$

where $e^j$ is the unit vector of the normal wave polarization ($j = 1,2$), and $\mathcal{N}_{sn}$ is the number density of the atoms in the state $|0, s, n\rangle$. The polarizations can be determined (Pavlov et al. 1980) from the polarizability tensor of the medium. The polarizability of the atomic component in a strong magnetic field has not yet been investigated even for the simplest case of hydrogen atoms. However, one can anticipate that at $\hbar\omega_B \gg$ Ry and $\omega_B \gg \omega$ the normal waves should be polarized almost linearly in a wide range of wave vector directions outside a narrow cone around $\boldsymbol{B}$, as in the case of a fully ionized plasma. In this "quasi-transverse" approximation the absorption coefficients of the "extraordinary" ($e^1 \perp \boldsymbol{B}$) and "ordinary" ($e^2$ in the $[\boldsymbol{Bq}]$-plane) waves are

$$k_1 = \frac{k_{+1+1} + k_{-1-1}}{2} - \mathrm{Re}\, k_{+1-1} , \quad (45)$$

$$k_2 = k_{00} \sin^2\theta + \frac{k_{+1+1} + k_{-1-1}}{2} \cos^2\theta + \mathrm{Re}\left(k_{+1-1} \cos^2\theta - \frac{k_{+10} + k_{-10}}{\sqrt{2}} \sin 2\theta\right) . \quad (46)$$

These equations can be further simplified in the dipole approximation, when $k_{\mu\nu} = k_{\mu\mu}\delta_{\mu\nu}$, and $k_{\mu\mu}$ is independent of $\theta$. The absorption of the extraordinary wave is isotropic in this approximation, whereas $k_2(\theta = \pi/2) \gg k_2(\theta = 0)$. Since the cross sections for the transverse polarizations ($\mu, \nu = \pm 1$) are much smaller than for the longitudinal one at $\omega \ll \omega_B$, the extraordinary photons have a longer mean free path in a wide range of $\vartheta$, thus determining the properties of radiation escaping from an optically thick medium. This means that an accurate evaluation of $\sigma^{+1+1}_{0sn}$ and $\sigma^{-1-1}_{0sn}$ is especially important, and using the velocity form of the interaction matrix elements in the adiabatic approximation is inappropriate because it leads to zero absorption of the extraordinary mode.

Besides an investigation of the normal wave polarizations, three more problems should be solved for incorporating the photoionization into modeling realistic neutron star atmospheres. *First*, it would be desirable to calculate the cross sections, particularly those for the transverse polarizations, outside the framework of the adiabatic approximation, i.e., to take into account the admixture of the states with different $N$ to the initial and final states. *Second*, one should take into account the effect of the atomic motion on the photoionization. The motion across the magnetic field generates the Lorentz electric field, $\boldsymbol{E} = c^{-1}\boldsymbol{v} \times \boldsymbol{B}$, which breaks the axial symmetry, leading thereby to distortion of the atomic structure, violation of the selection rules, additional shifts and smoothing of the ionization thresholds, and alteration of the cross section magnitudes. *Third*, since the atmospheres of neutron stars are much denser than those of usual stars, the opacities should be calculated with allowance for pressure effects which partly destroy the discrete states (Ventura et al. 1992) of the atom and lead to additional smoothing of the ionization thresholds.

We are grateful to Joseph Ventura and Peter Mészáros for useful discussions. We are also pleased to acknowledge helpful referee's comments of Heinz Herold. This research has been supported in part through NASA grant NAGW-1522.

## APPENDIX A

## INTERACTION MATRIX ELEMENTS

Interaction between a hydrogen atom and a photon with the wave vector $\boldsymbol{q}$ and frequency $\omega$ is described by the following potential

$$H_{\mathrm{int}} = e\sqrt{\frac{2\pi\hbar}{\omega}} \left\{\exp(i\boldsymbol{q}\boldsymbol{r}_e) \frac{\boldsymbol{\pi}_e \cdot \boldsymbol{e}}{m_e} - \exp(i\boldsymbol{q}\boldsymbol{r}_p) \frac{\boldsymbol{\pi}_p \cdot \boldsymbol{e}}{m_p}\right\} , \quad (A1)$$

where

$$\boldsymbol{\pi}_{e,p} = -i\hbar\nabla_{\boldsymbol{r}_{e,p}} \pm \frac{e}{2c} \boldsymbol{B} \times \boldsymbol{r}_{e,p} = \frac{m_{e,p}}{M}\left(\boldsymbol{P} + \frac{e}{c}\boldsymbol{B} \times \boldsymbol{r}\right) \pm \left(\boldsymbol{\pi} + \frac{e}{2c}\boldsymbol{B} \times \boldsymbol{R}\right) \quad (A2)$$

are the kinetic momenta of the electron (subscript "$e$," upper signs) and the nucleus (subscript "$p$," lower signs), $\boldsymbol{r}_{e,p}$ denote their positions, $\boldsymbol{r} = \boldsymbol{r}_e - \boldsymbol{r}_p$, $\boldsymbol{R} = (m_p\boldsymbol{r}_p + m_e\boldsymbol{r}_e)/M$; $\boldsymbol{P}$ and $\boldsymbol{\pi}$ are given by equations (2) and (4). The matrix element of the interaction potential between the states $\Psi$ and $\Psi_f$ (see eq. [1]) is equal to

$$\langle\Phi_f | H_{\mathrm{int}} | \Psi\rangle = ie\sqrt{2\pi\hbar\omega}\,(\boldsymbol{D} \cdot \boldsymbol{e})(2\pi)^3\delta(\boldsymbol{K}_f - \boldsymbol{K} - \boldsymbol{q}) , \quad (A3)$$

where $\hbar\boldsymbol{K}$ and $\hbar\boldsymbol{K}_f$ are the eigenvalues of $\boldsymbol{P}$,

$$\boldsymbol{D} = (i\omega)^{-1}\langle\psi_f | A_0^-[\hbar\boldsymbol{K} + (e/c)\boldsymbol{B} \times \boldsymbol{r}]/M + A_1^+ \boldsymbol{\pi}/\mu | \psi\rangle \equiv \boldsymbol{D}^{(\pi)} , \quad (A4)$$

$$A_n^{\pm} = (m_p/M)^n \exp(im_p\boldsymbol{q} \cdot \boldsymbol{r}/M) \pm (m_e/M)^n \exp(-im_e\boldsymbol{q} \cdot \boldsymbol{r}/M) .$$

Making use of the commutation relations

$$[\mathrm{H}_K, \boldsymbol{r}] = (\hbar/i\mu)\boldsymbol{\pi} , \tag{A5}$$

$$[H_K, e^{i\boldsymbol{k}\boldsymbol{r}}] = e^{i\boldsymbol{k}\boldsymbol{r}}(\hbar^2k^2/2\mu + \hbar\boldsymbol{k}\cdot\boldsymbol{\pi}/\mu) , \tag{A6}$$

where $H_K$ is given by equation (3), one can transform the velocity form of the matrix element (A4) to the length form

$$\boldsymbol{D} = \langle\psi_f|\boldsymbol{r}\left\{A_1^+\left[1 - \frac{\boldsymbol{q}\cdot(\hbar c\boldsymbol{K} + e\boldsymbol{B}\times\boldsymbol{r})}{M\omega c}\right] - A_2^+\frac{\hbar q^2}{2\mu\omega} - A_2^-\frac{\boldsymbol{q}\cdot\boldsymbol{\pi}}{\mu\omega}\right\} - iA_1^-\frac{\hbar c\boldsymbol{K} + e\boldsymbol{B}\times\boldsymbol{r}}{M\omega c}|\psi\rangle \equiv \boldsymbol{D}^{(r)} . \tag{A7}$$

Equations (A4) and (A7) are valid for arbitrary momentum of the atom, ratio $m_e/m_p$, and relation between the radiation wavelength and atomic dimensions. They are simplified substantially in the dipole approximation ($\boldsymbol{q} \to 0$),

$$\boldsymbol{D}^{(\pi)} = (i\omega\mu)^{-1}\langle\psi_f|\boldsymbol{\pi}|\psi\rangle , \tag{A8}$$

$$\boldsymbol{D}^{(r)} = \langle\psi_f|\boldsymbol{r}|\psi\rangle , \tag{A9}$$

and for $m_p/m_e \to \infty$,

$$\boldsymbol{D}^{(\pi)} = (im_e\omega)^{-1}\langle\psi_f|\exp(i\boldsymbol{q}\boldsymbol{r})\boldsymbol{\pi}|\psi\rangle , \tag{A10}$$

$$\boldsymbol{D}^{(r)} = \langle\psi_f|\boldsymbol{r}\exp(i\boldsymbol{q}\boldsymbol{r})\left(1 - \frac{\hbar q^2}{2m_e\omega} - \frac{\boldsymbol{q}\cdot\boldsymbol{\pi}}{m_e\omega}\right)|\psi\rangle . \tag{A11}$$

The velocity and length forms of the matrix element $\boldsymbol{D}$ would be equivalent if $\psi_f$ and $\psi$ were exact wave functions. However, if one applies the adiabatic approximation (7), these forms may lead to qualitatively different results. This can be demonstrated in the most transparent way for the case $m_p/m_e \to \infty$ in the adiabatic dipole approximation. In this case the circular components of $\boldsymbol{D}$, $D_{\pm1} \equiv (D_x \pm iD_y)/2^{1/2}$, take the form

$$D_{\pm1}^{(\pi,\mathrm{ad})} = (i\omega m_e)^{-1}\langle\psi_f^{\mathrm{ad}}|\pi_{\pm1}|\psi^{\mathrm{ad}}\rangle = \mp a_L\frac{\omega_B}{\omega}\sqrt{N_{\max}}\,\delta_{N_f,N\pm1}\,\delta_{s_f,s\mp1}\langle g_f|g\rangle \tag{A12}$$

and

$$D_{\pm1}^{(r,\mathrm{ad})} = \langle\psi_f^{\mathrm{ad}}|r_{\pm1}|\psi^{\mathrm{ad}}\rangle = a_L(-\sqrt{N_{\max}}\,\delta_{N_f,N\pm1} + \sqrt{N + s_{\max}}\,\delta_{N_f,N})\delta_{s_f,\mp1}\langle g_f|g\rangle , \tag{A13}$$

where $N_{\max} = \max(N, N_f)$, $s_{\max} = \max(s, s_f)$, and $\psi^{\mathrm{ad}}$ is defined by equation (8). Equations (A12) and (A13) yield the relation

$$D_{\pm1}^{(\pi,\mathrm{ad})} = D_{\pm1}^{(r,\mathrm{ad})}(N_f - N)\omega_B/\omega . \tag{A14}$$

The most striking discrepancy takes place in the most important case $N_f = N$, when $D_{\pm1}^{(r,\mathrm{ad})} \neq 0$, whereas $D_{\pm1}^{(\pi,\mathrm{ad})}$ vanishes identically.

It seems clear that vanishing $D_{\pm1}^{(\pi,\mathrm{ad})}$ at $N_f = N$ is caused solely by the adiabatic approximation, and the nonzero value of $D_{\pm1}^{(r,\mathrm{ad})}$ can be considered at least as an approximate evaluation of the matrix element. To verify consistency of this assumption, let us suppose that at some $\omega$ the adiabatic approximation for the wave functions (see eq. [7]) holds also for longitudinal matrix elements, i.e.,

$$\langle g_{N's'}|h_{N''}^{Ns}\rangle = O(\epsilon\langle g_{N's'}|g_{Ns}\rangle) , \qquad \epsilon \ll 1 , \tag{A15}$$

and find the first correction to $D_{\pm1}^{(\pi,\mathrm{ad})}$. Applying equation (9) and the equality

$$\langle\Phi_{N_fs_f}|\pi_{\pm1}|\Phi_{Ns}\rangle = im_e(N_f - N)\omega_B\langle\Phi_{N_fs_f}|r_{\pm1}|\Phi_{Ns}\rangle , \tag{A16}$$

one obtains

$$D_{\pm1} - D_{\pm1}^{(\pi,\mathrm{ad})} = \pm\frac{\omega_B}{\omega}\{(1 - \delta_{N_f,N\pm1})(\langle\Phi_{N\pm1,s_f}|r_{\pm1}|\Phi_{N_s}\rangle\langle h_{N\pm1}^{N_fs_f}|g_{Ns}\rangle - (\langle\Phi_{N_fs_f}|r_{\pm1}|\Phi_{N_f\mp1,s}\rangle\langle g_{N_fs_f}|h_{N_f\mp1}^{Ns}\rangle) + O(\epsilon^2)\} . \tag{A17}$$

On the other hand, it follows from the assumption (A15) that $D_{\pm1} = D_{\pm1}^{(r,\mathrm{ad})} + O(\epsilon)$. Thus, with allowance for equation (A14), one obtains

$$D_{\pm1} - D_{\pm1}^{(\pi,\mathrm{ad})} = \left\{1 - (N_f - N)\frac{\omega_B}{\omega}\right\}\langle\Phi_{N_fs_f}|r_{\pm1}|\Phi_{Ns}\rangle\langle g_{N_fs_f}|g_{Ns}\rangle + O(\epsilon) . \tag{A18}$$

Equations (A17) and (A18) are consistent with equation (A15), if only

$$|\omega - (N_f - N)\omega_B| \ll \omega_B . \tag{A19}$$

Violation of the condition (A15) outside this frequency range can be also shown directly from a set of the differential equations for $g(z)$ and $h(z)$ (see, e.g., Simola & Virtamo 1978), making use of explicit form of nondiagonal Coulomb matrix elements which couple these equations. Thus, the length form in the adiabatic approximation is justified just above the Landau thresholds, where the cross sections are maximal, including the most important region $\omega \ll \omega_B$ which realizes at $N_f = N$ only (i.e., above the "zeroth"

threshold). Equation (A17) shows clearly that the velocity form does not work in this region, whereas both forms coincide approximately if $N_f \neq N$ and the condition (A19) is fulfilled. On the contrary, the two forms differ essentially outside the frequency regions (A19), i.e., below the Landau thresholds, but violation of the assumption (A15) in this case indicates, strictly speaking, that the adiabatic approximation is inapplicable with both forms. Nevertheless, since it occurs at frequencies where the cross section itself is comparatively low, we may expect that deviations of the exact cross sections from the adiabatic ones will not be too important for astrophysical applications.

Note that all these problems arise for the transverse components $D_{\pm 1}$ only as the velocity and length forms coincide for the longitudinal component, $D_0^{(\pi,\mathrm{ad})} = D_0^{(r,\mathrm{ad})}$, if the Schrödinger equation for $g_{N_s}(z)$ is solved accurately.

## APPENDIX B

## TECHNICALITIES OF COMPUTATION

### 1. EFFECTIVE POTENTIALS

It follows from equation (10) and properties of the functions $\Phi_{Ns}(\rho, \phi)$ (see eq. [5]) that $v_{Ns}(\zeta) = v_{n_\rho|s|}(|\zeta|)$ with $n_\rho \equiv N + (s - |s|)/2$, and each $v_{Ns}(\zeta)$ is a linear combination of the functions $v_{0s'}(\zeta)$ with $s' = |s|, |s| + 1, \ldots, |s| + 2n_\rho$. All these functions can be reduced to $v_{00}(\zeta) = \pi^{1/2} \exp(\zeta^2) \operatorname{erfc}(\zeta)$ with the aid of recurrence relations (see, e.g., Alijah et al. 1990). The function $v_{00}(\zeta)$ can be computed very fast and accurate making use of the rational approximation of erfc $(\zeta)$ at $|\zeta| < 1$ and the continued-fractions expansion at $\zeta \geq 1$ (Abramovitz & Stegun 1972). The recurrence from $v_{0s}$ to $v_{00}$ loses stability at large $\zeta$ and $s$ due to increasing round-off errors. In this case the asymptotic expansion

$$v_{0s}(\zeta) = \frac{1}{\sqrt{\zeta^2 + s + p}} \left\{ 1 - \frac{1}{2} \frac{1-p}{\zeta^2 + s + p} + \frac{3}{8} \frac{s + 1 + (1-p)^2}{(\zeta^2 + s + p)^2} - \cdots \right\} \tag{B1}$$

can be applied, where $p$ is an arbitrary parameter. Rösner et al. (1983) used the value $p = \frac{1}{2}$. We use $p = 1$ as it minimizes the numerators of the second and third terms in equation (B1). To estimate the potentials for $N > 0$ at large $\zeta$, one can also use the relation

$$v_{n_\rho|s|}(\zeta) \sim (\zeta^2 + 2n_\rho + |s| + 1)^{-1/2}, \tag{B2}$$

which is valid at large $\zeta$.

### 2. WAVE FUNCTIONS OF THE DISCRETE SPECTRUM

The eigenvalues $\epsilon = -\epsilon_{0sn}$ and eigenfunctions $g_{0sn}$ are computed with three nested iterations. Within the inner iteration, equation (29) is integrated and the estimate $\hat{\epsilon}_{0sn}$ is varied so as to meet desired boundary conditions and the number of nodes for the function $g(\zeta)$. Within two outer iterations, the integration length and the number of mesh points are varied. The boundary conditions are imposed and integration is carried out following the procedure described by Simola & Virtamo (1978). We, however, apply the Runge-Kutta (instead of "predictor-corrector") method and the nonuniform mesh, $\zeta_j = hj^2, j = 0, \ldots, J$, which is more convenient concerning slower variation of $g(\zeta)$ at large $\zeta$. The starting value $\hat{\epsilon}_{0sn}$ is taken in accordance with the asymptotic estimation at large $\beta$, the starting length $\zeta_J$ is taken near the classical turning point, and the starting number $J$ is taken so as the initial integration step is less than unity. The normalizing integral is computed with adding asymptotic extension of $g(\zeta)$ in the region $\zeta > \zeta_J$. The procedure is terminated when the difference between estimations $\hat{\epsilon}_{0sn}$ at the successive iterations is less than 0.1%.

### 3. WAVE FUNCTIONS OF THE CONTINUUM

Equation (29) at $\epsilon > 0$ has the solutions $g_\pm(\zeta)$ which behave as $\exp[\pm i\epsilon/(\beta)^{1/2}\, \zeta + i \ln|\zeta|/\epsilon^{1/2}]$ at $\zeta \to \mp\infty$. These functions describe the states in which the outcoming wave is absent. In analogy to the three-dimensional case, one should use the functions $g_\pm(\zeta)$ with definite momentum directions at infinity. However, for computing the total cross section summed over the final momenta one can use a set of real symmetric and antisymmetric wave functions, $g_s(\zeta)$ and $g_a(\zeta)$, which behave at infinity as $\cos[\epsilon/(\beta)^{1/2}\, \zeta + \operatorname{sign}\zeta \times \ln|\zeta|/\sqrt{\epsilon} + \chi)$, with $\chi = \chi_s$ or $\chi_a$, respectively. In the dipole approximation, a nonzero contribution to the cross section comes from only one of the two functions, depending on parity of the initial state $(0sn)$.

To compute the functions $g_s$ and $g_a$, we apply the Runge-Kutta scheme in the region $|\zeta| < \zeta_{\max}$ which gives the main contribution to the matrix elements. The value of $\zeta_{\max}$ depends on $s$, $n$, and $\epsilon_f$; in particular, oscillations of the integrand increase $\zeta_{\max}$ significantly at $\epsilon_f \gg \epsilon_{0sn}$. The wave functions are normalized by comparing with the asymptotic expressions. At small $\epsilon_f$, the function $g(\zeta)$ approaches the large-distance asymptotes very slowly. In this case, solving equation (29) is extended to large $\zeta$ by a stable less-order scheme with a larger step of integration.

### 4. MATRIX ELEMENTS

To calculate the matrix elements, we choose a variable step of integration equal to the minimum of those used for calculation of corresponding bound-state and continuum wave functions. For calculation of each next term in the integral sum, the functions are approximated by cubic polynomials with coefficients providing correct values of the function and its first derivative at two nearest mesh points. To save the computer time and memory, the matrix elements are calculated simultaneously with the continuum wave functions.

REFERENCES

Abramowitz, M., & Stegun, I. A. 1972, Handbook of Mathematical Functions (New York: Dover)
Alijah, A., Hinze, J., & Broad, J. T. 1990, J. Phys. B, 23, 45
Bhattacharya, S. K., & Chu, S.-I. 1985, J. Phys. B, 18, L275
Canuto, V., & Ventura, J. 1977, Fund. Cosmic Phys., 2, 203
Delande, D., Bommier, A., & Gay, J. C. 1991, Phys. Rev. Lett., 66, 141
Forster, H., Strupat, W., Rösner, W., Wunner, G., Ruder, H., & Herold, H. 1984, J. Phys. B, 17, 1301
Garstang, R. H. 1977, Rep. Prog. Phys., 40, 105
Gnedin, Yu. N., & Pavlov, G. G. 1974, Soviet Phys.—JETP, 38, 903
Gnedin, Yu. N., Pavlov, G. G., & Tsygan, A. I. 1974, Z. Eksper. Teoret. Fiz., 66, 421 (Soviet Phys.—JETP, 39, 301)
Gor'kov, L. P., & Dzialoshinskii, I. E. 1967, Z. Eksper. Teoret. Fiz., 53, 717
Greene, C. H. 1983, Phys. Rev. A, 28, 2209
Hasegawa, H., & Howard, R. E. 1961, J. Phys. Chem. Solids, 21, 179
Herold, H., Ruder, H., & Wunner, G. 1981, J. Phys. B, 21, 447
Kaminker, A. D., & Yakovlev, D. G. 1981, Teor. Matem. Fiz., 49, 248
Kara, S. M., & McDowell, M. R. C. 1981, J. Phys. B, 14, 1719
Mega, C., Herold, H., Rösner, W., Ruder, H., & Wunner, G. 1984, Phys. Rev. A, 30, 1507
Miller, M. C., & Neuhauser, D. 1991, MNRAS, 253, 107
Pavlov, G. G., Shibanov, Yu. A., & Yakovlev, D. G. 1980, Ap&SS, 73, 33
Rösner, W., Herold, H., Ruder, H., & Wunner, G. 1983, Phys. Rev. A, 28, 2071
Rösner, W., Wunner, G., Herold, H., & Ruder, H. 1984, J. Phys. B, 17, 29
Schmitt, W., Herold, H., Ruder, H., & Wunner, G. 1981, A&A, 94, 194
Simola, J., & Virtamo, J. 1978, J. Phys. B, 11, 3309
Sokolov, A. A., & Ternov, I. M. 1968, Synchrotron Radiation (Berlin: Akademie-Verlag)
Ventura, J., Herold, H., Ruder, H., & Geyer, F. 1992, A&A, 261, 235
Wunner, G., Herold, H., & Ruder, H. 1983a, J. Phys. B, 16, 2937
Wunner, G., Ruder, H., Herold, H., & Schmitt, W. 1983b, A&A, 117, 156